Preprints (www.preprints.org) | NOT PEER-REVIEWED | Posted: 30 July 2021

Article

Luminescence sensitivity of Rhine valley loess: indicators of source variability?

Kathryn E. Fitzsimmons [1,2]*, Zoran Perić [1], Maike Nowatzki [1,3], Susanne Lindauer [4], Mathias Vinnepand [5], Charlotte Prud'homme [1,6], Aditi K. Dave [1], Andreas Vött [5] and Peter Fischer [5]

[1] Research Group for Terrestrial Palaeoclimates, Max Planck Institute for Chemistry, 55128 Mainz, Germany; k.fitzsimmons@mpic.de; z.peric@mpic.de
[2] Department of Geosciences, University of Tübingen, 72076 Tübingen, Germany; k.fitzsimmons@uni-tuebingen.de
[3] School of Geography and the Environment, University of Oxford, OX1 3QY Oxford, UK; maike.nowatzki@ouce.ox.ac.uk
[4] Curt-Engelhorn-Centre for Archaeometry, 68159 Mannheim, Germany; susanne.lindauer@ceza.de
[5] Institute of Geography, Johannes Gutenberg University Mainz, 55128 Mainz, Germany; a.voett@geo.uni-mainz.de, p.fischer@geo.uni-mainz.de
[6] Institute of Earth Surface Dynamics, University of Lausanne, 1015 Lausanne, Switzerland; charlotte.prudhomme@unil.ch
* Correspondence: k.fitzsimmons@mpic.de; k.fitzsimmons@uni-tuebingen.de

Abstract:
Loess provides a valuable terrestrial record of past environmental conditions, including the dynamics of air mass circulation responsible for dust transport. Here we explore variations in the luminescence characteristics of sedimentary quartz and feldspar – dominant minerals in loess-palaeosol sequences (LPS) - as possible tools for identifying changes in source. We investigate luminescence sensitivity, a rapidly measurable index which is the product of interplay between source lithology and the history of the mineral in question. Variations in sensitivity down profile may therefore reflect, among other factors such as pedogenesis and reworking, changes in sediment provenance. We undertake an empirical investigation of the luminescence sensitivity of quartz and feldspar from different grain-size fractions from the climatically sensitive Schwalbenberg LPS in the German Rhine valley, comparing samples from a 30 m core spanning the last full glacial cycle with samples of oxygen isotope stage (OIS) 3-2 age exposed within a c. 6 m profile downslope. The temporal overlap enables comparison of luminescence characteristics with respect to possible provenance change during that timeframe. We find an overall inverse relationship between quartz and feldspar sensitivity, as well as variability in sensitivity between different quartz grain sizes. There is some indication that feldspar sensitivity increases during periods of soil formation down the core. In particular, measurements of IR_{50} sensitivity on unprocessed sediments show correlation with down-profile trends in more established indicators of provenance. This suggests it may be used to provide a reliable, rapid scan of sensitivity changes, and may suggest source variability over millennial timescales.

Keywords: loess-palaeosol sequences, luminescence signal sensitivity, quartz, feldspar, Schwalbenberg, sediment provenance, sediment history, optically stimulated luminescence, infrared stimulated luminescence, Central Europe, Rhine valley

© 2021 by the author(s). Distributed under a Creative Commons CC BY license.

Preprints (www.preprints.org) | NOT PEER-REVIEWED | Posted: 30 July 2021

1. Introduction

Loess – a homogeneous, permeable, predominantly silt-sized aeolian sediment [1, 2] – has long been recognised as a valuable terrestrial record of past environmental conditions [3-5]. Loess deposits drape some 10% of the Earth's land surface, predominantly in the dry subhumid to semi-arid temperate latitudes [6], accumulating almost continuously for more than one million years in some regions [7-9]. It is assumed that classical stacked loess-palaeosol-sequences (LPS) represent deposition and in situ weathering in response to cooler glacial/stadial and warmer interglacial/interstadial climates respectively [4, 5, 10]. Most aeolian dust is thought not to travel far, often deriving from fine-grained material transported by rivers from glaciated regions [11-13], although distal transport is also widely acknowledged [e.g. 14, 15]. Loess deposits are implicitly linked with the pathways of major air masses thought to transport the dust [e.g. 16, 17].

The provenance of loess sediment, and how this may have changed through time over the history of a deposit, is inferred from the trajectories and dynamics of atmospheric circulation systems [e.g. 18, 19, 20]. The most frequently used techniques for correlating aeolian dust deposits with likely source areas include bulk geochemistry [16, 21-23], the age distribution profiles of detrital zircons [24-26], and Sr-Nd isotope ratios [15, 27, 28]. However, each of these approaches is limited in the information they may provide about loess provenance. Whilst in some instances bulk geochemistry can identify dust source changes due to variations in atmospheric circulation (such as a shift from mafic to felsic catchment source; see [29]), unequivocal links between source and sink can rarely be effectively identified because of homogenisation during transport [23, 27]. Detrital zircons are limited in utility due to age overlap and variable zircon fertility within source rocks [25]. Radiogenic isotopes are limited to identifying the origins of clay minerals rather than the more dominant silt-sized quartz and feldspar [27].

Since loess is dominated by silicate minerals – namely, quartz and feldspars - it is advantageous to explore their potential as indicators of source changes within LPS. Increasingly, researchers have been exploring variations in the luminescence characteristics of sedimentary quartz and feldspar as possible provenance tools [30-32]. Most investigations have focussed on quartz by virtue of its less complex crystalline framework. Approaches include cathodoluminescence signal spectra deriving from crystalline impurities which relate to source rock formation [33, 34]; electron spin resonance (ESR) signal intensity of luminescence centres which are thought to reflect source rock age [34, 35]; ratios of linearly-modulated optically stimulated luminescence (OSL) components as proxies for formation age [36, 37]; and OSL sensitivity measurements as a qualitative indicator of source lithology and transport history [38-41]. Of these approaches, OSL sensitivity is the quickest to measure and has therefore been favoured in loess studies as a means to rapidly assess potential changes in sediment source down LPS profiles [42-44].

OSL sensitivity – the signal intensity per absorbed radiation dose – arises from the efficiency of charge traffic between traps and luminescence centres within a crystalline framework [45]. In a sedimentary context, sensitivity is the product of interplay between source lithology and the history of the mineral in question [32], including sedimentary history, extrusion/deposition and metamorphosis. Consequently, shifts in sediment provenance may be observed through variations in OSL sensitivity down LPS [43]. Other, additional luminescence characteristics such as dose

Preprints (www.preprints.org) | NOT PEER-REVIEWED | Posted: 30 July 2021

recovery [44] and infrared stimulated luminescence (IRSL):OSL ratios [42] have also been observed to change in parallel, but require additional measurements. OSL sensitivity profiles have so far been generated for LPS sites on the Chinese Loess Plateau [43, 44] and in Central Asia [42]. Despite the presence of thick loess deposits across Europe [3, 46, 47, 48], however, this approach has yet to be tested on that continent.

Here we undertake an empirical investigation of the luminescence sensitivity characteristics of quartz and feldspar from different grain-size fractions at the Schwalbenberg LPS in the German Rhine valley. In doing so we test the potential of luminescence sensitivity as an indicator of changes in sediment source through time. Although feldspar, as a solid solution, exhibits substantially more complexity in its crystalline framework and recombination mechanisms than does quartz [e.g. 49-52], we undertake the first step towards exploring the potential of feldspar luminescence sensitivity for this purpose in the form of an empirical study. We compare samples collected from a 30 m core spanning the last full glacial cycle at high resolution [53, 54], with samples of oxygen isotope stage (OIS) 3-2 age exposed within a c. 6 m profile on the southern margins of the Schwalbenberg deposit [53]. The temporal overlap of the two localities during OIS3 enables comparison of luminescence characteristics with respect to possible shifts in provenance during that timeframe.

2. Materials and Methods

2.1 Sampling site

This study focusses on the loess deposits of the Schwalbenberg site, located west of the city of Remagen and just north of the confluence between the rivers Ahr and Rhine in western Germany (Figure 1). Loess deposits up to 30 m thick drape the fluvial terraces of the Rhine, and Devonian sedimentary bedrock [53, 55], providing some of the thickest and most complete deposits in western Europe [56, 57]. The loess deposits at Schwalbenberg have been the focus of a number of studies describing the stratigraphy and sediments, including their chemistry, in detail. Most studies investigated and excavated profiles exposed along the margins of the hillslope, with the antiquity of the deposits inferred through correlation [e.g. 55, 58-62]. More recently, four cores (REM 1, 3A/3B, 5) were drilled and sampled across the hillslope in order to reconstruct palaeoenvironmental change in four dimensions based on physical characteristics and geochemistry [53-55].

Preprints (www.preprints.org) | NOT PEER-REVIEWED | Posted: 30 July 2021

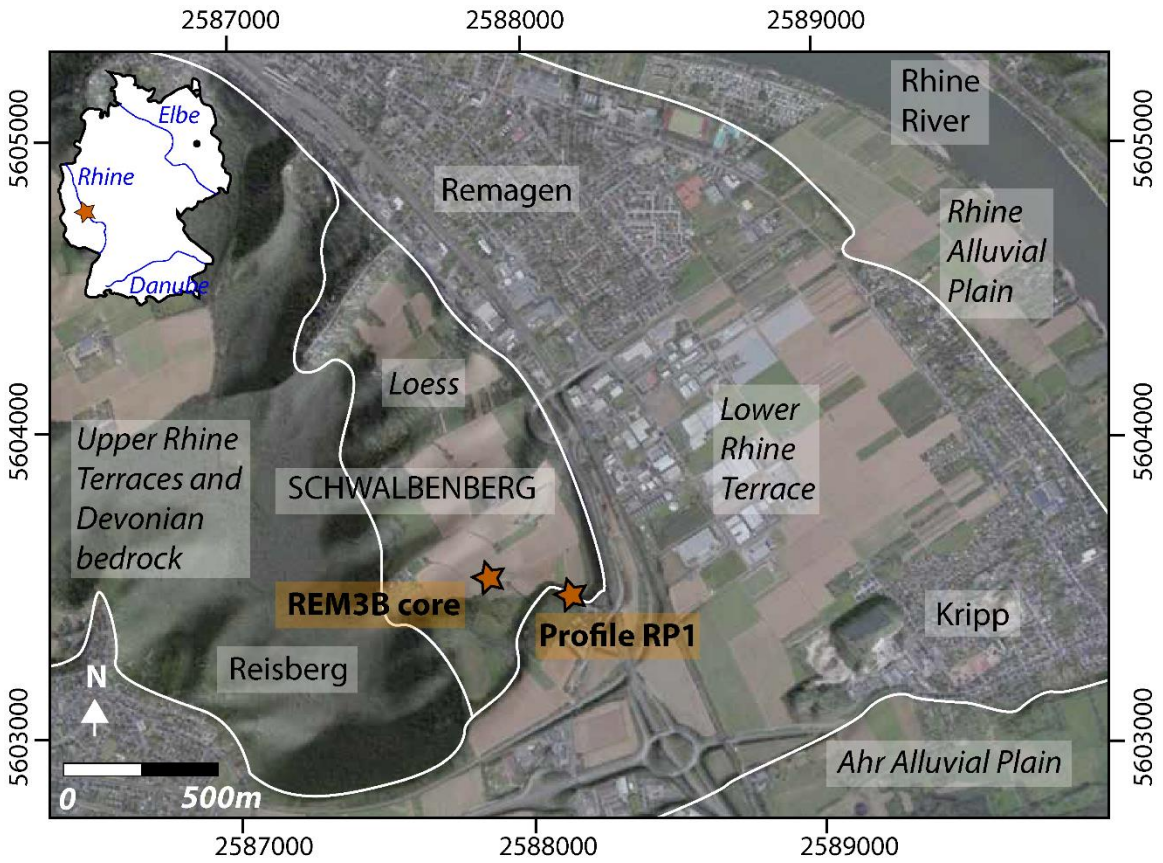

Figure 1. Location of the Schwalbenberg site, west of the Rhine River and southwest of the city of Remagen (position within Germany shown in inset). The locations of the REM3B core and profile RP1 are shown by orange stars. Prominent breaks in slope are highlighted in white. The map is based on data from the digital elevation model (DGM 5), Geobasisdaten, Landesvermessungsamt Rheinland-Pfalz and Microsoft Bing Maps.

In this study, we focus on two sets of samples collected from the Schwalbenberg locality. Firstly, we sampled the upper 25 m of the 30 m long REM3B core. Fluvial sediments unrelated to the loess sequence dominate depths below 25 m and were beyond the scope of interest here. The REM3B core was collected adjacent the REM3A core described in [54], and was collected in order to facilitate luminescence dating for chronological control. Stratigraphic correlations suggest the REM3 cores to span the last full glacial cycle [53]. The basal metres comprise fluvial sandy silts, with some gravels, correlated based on elevation to the Rhine terraces of last interglacial age and earlier [62]. In addition, we collected four samples from a c. 6 m thick loess profile, RP1, situated on the southern margins of the hill and approximately 200 m west of the previously described sections [57, 59, 60, 62]. Loess at RP1 accumulated over late OIS3 into OIS2 [53]. This chronology is based on radiocarbon dating of molluscs [65] and earthworm calcite granules [53], as well as luminescence dating using quartz OSL and polymineral post-infrared infrared stimulated luminescence (pIR-IRSL) on multiple grain-size fractions [53].

2.2 Luminescence measurements on the RP1 profile

Four luminescence samples were collected from profile RP1 for the dating analysis described in [53]. These samples were treated to isolate sand-sized (100-200 μm) and very fine sand-sized (63-100 μm) quartz for OSL dating, according to availability and using published methods [66]. These size fractions were loaded as 14-24 small aliquots (50-100 grains each) onto stainless steel discs for

Preprints (www.preprints.org) | NOT PEER-REVIEWED | Posted: 30 July 2021

measurement (Table S1). Eighteen aliquots of fine-grained (4-11 μm) polymineral material were additionally prepared from each sample according to [66].

All luminescence measurements were made on an automated Risø TL-DA-12 reader using blue-green or infrared light-emitting diodes (LEDs) to excite the OSL and IRSL/pIR-IRSL signals respectively [65]. Measurements were undertaken in the luminescence dating laboratory of the Curt Engelhorn Zentrum für Archaeometrie (CEZA) in Mannheim. Quartz OSL measurements for De were undertaken using the single aliquot regenerative dose (SAR) protocol of Murray and Wintle [68, 69], using preheat and cutheat temperatures of 240°C and 220°C respectively and applying four regenerative dose steps. The pIR-IRSL protocol [72] was applied to the polymineral fine-grained samples using an initial IRSL measurement temperature of 50°C and pIR-IRSL measurement temperature of 290°C (and is henceforth designated as $pIR_{50}IRSL_{290}$). D_e values calculated for the RP1 samples are listed in Table S2 and described in more detail in [53]. While not all aliquots exhibited characteristics acceptable for dating, we focus here on the luminescence sensitivity of all aliquots measured, which produced signal suitable for sensitivity calculations. These were calculated from the luminescence signal arising from the test dose immediately following measurement of the natural signal, and are quantified in counts/second/Gy [38].

2.2 Luminescence measurements on the REM3B core

Core REM3B was split lengthwise for sampling under subdued red light conditions. One half of the core was sampled at semi-regular intervals for D_e preparation and measurement, and the other half was sampled at the same depths for dose rate analysis to facilitate eventual age calculations. The stratigraphy of the core was logged and correlated with the adjacent core REM3A to produce a composite core REM3 (described in [53]; Figure S1). A total of 102 samples were collected at high frequency down core REM3B, each comprising ten vertical centimetres of sediment accumulation; five samples derived from the basal fluvial units and are hereafter disregarded from further consideration in this study, since the focus is on the aeolian sediments. All REM3B core samples and their depths are listed in the Supplementary Information (Table S3).

We investigated luminescence signals and sensitivity using IRSL on 83 samples down the column; $pIR_{50}IRSL_{290}$ on 8 samples between c. 1.3-3.5 depth; $pIR_{200}IRSL_{290}$ (using a higher initial IRSL temperature of 200°C) on 11 samples between 3.5-16.6 m depth; and OSL of two different size fractions for samples collected between 3.5-6.5 m and the lowermost 7 m respectively (Table S3). The post-IR-IRSL measurements were all undertaken on 63-100 μm processed and density-separated material and therefore comprises K-feldspar rather than polymineral, as was the case for the fine-grained aliquots measured from the profile RP1. All luminescence measurements were made on automated Risø TL-DA-20 readers using blue-green or infrared light-emitting diodes (LEDs) to excite the OSL and IRSL/pIR-IRSL signals respectively [67]. Measurements were undertaken in the luminescence dating laboratory at the Max Planck Institute for Chemistry (MPIC), Mainz.

We first undertook a rapid assessment of IRSL signal increase with depth, and corresponding sensitivity, on 83 unprocessed samples down core REM3B. Three aliquots of unprocessed, unexposed sediment per sample were pipetted onto stainless steel discs for measurement of the natural $IRSL_{50}$

Preprints (www.preprints.org) | NOT PEER-REVIEWED | Posted: 30 July 2021

signal (L_n) at 50°C, followed by a test dose of approximately 37 Gy, and measurement of the $IRSL_{50}$ signal following that test dose (T_n). We selected a constant test dose that was the same as that applied to the RP1 samples to ensure consistency for the sample suite.

Following the initial $IRSL_{50}$ scans, selected samples from regular intervals were treated to isolate very fine sand-sized (63-90 μm) and very fine silt (4-11 μm) material according to published methods for core samples [71]. Five very fine sand-sized (63-100 μm) samples from the depth range c. 3.5-6.5 m were subsampled for extraction of both purified quartz and K-feldspar signal measurement, and 10 very fine silt-sized samples (4-11 μm) from >23 m depth were processed for quartz. The subsamples for quartz purification were etched in fluorosilicic acid according to published methods [72]. Following insights from earlier studies indicating that quartz signals in Remagen loess rarely yield reliable ages [55], we focused solely on processing and measurement of K-feldspar fractions for the remainder of the core. Six samples from the mid-lower part of the core (7.6-16.6 m) were processed solely for very fine sand-sized (63-100 μm) K-feldspar measurement.

We initially ran the $pIR_{200}IRSL_{290}$ protocol [70] on 6-12 aliquots of K-feldspar below 3.5 m depth. Following observation of the signal arising from these samples, we observed variable sensitivity between samples and aliquots. We therefore compared measurements from the $pIR_{200}IRSL_{290}$ protocol with those using the lower initial temperature $pIR_{50}IRSL_{290}$ protocol on sample A0379 (3.5 m depth) and found that the latter yielded more consistent results. Thereafter we measured the K-feldspar core samples above 3.5 m depth using the $pIR_{50}IRSL_{290}$ protocol on 24 aliquots each, with four regenerative dose points. Three aliquots each from the five 63-90 μm quartz samples were measured for OSL equivalent dose and sensitivity using the single aliquot regenerative dose (SAR) protocol [68, 69] using preheat and cutheat temperatures of 260°C and 240°C respectively, applying two regenerative dose steps and test doses of approximately 37 Gy. Three aliquots of each very fine silt-sized sample from the lowest part of the core were measured using the SAR protocol, applying preheat and cutheat temperatures of 260°C and 240°C respectively, three regenerative dose steps and test doses of approximately 37 Gy. Given the relatively small quantities of aliquots measured, mean equivalent doses are reported with 1σ uncertainty.

Additional tests for luminescence characteristics were run on the 63-100 μm K-feldspar fractions. Dose recovery in response to a laboratory-applied beta radiation dose of c. 100 Gy was measured on three K-feldspar aliquots of sample A0375 (4.45 m), and residual dose tests following bleaching under sunlight and under an LED lamp were measured on six aliquots each of samples A0375 and A0376 (4.45 m and 4.25 m depth respectively, bracketing the Eltville tephra; Table S4).

The luminescence sensitivities of the K-feldspar and quartz aliquots were calculated from the signal arising from the test dose immediately following measurement of the natural signal (T_n), divided by test dose size, and are quantified in counts/second/Gy [38].

3. Results

Whilst the focus of this study is on the luminescence sensitivity of different minerals and grain size fractions in the Schwalbenberg loess deposit, we also provide the approximate equivalent doses as a means of initially assessing the robustness of the age-depth relationships using the different

Preprints (www.preprints.org) | NOT PEER-REVIEWED | Posted: 30 July 2021

protocols. We therefore present our results in three parts: an overview of the equivalent dose measurements, followed by test-dose sensitivity data for the profile RP1 and the part of the core overlapping with RP1, and finally for the core REM3B.

3.1. Equivalent dose measurements

Most, but not all, aliquots of each respective measurement responded satisfactorily to the quartz OSL SAR or K-feldspar pIR-IRSL protocols. While signals from the $pIR_{200}IRSL_{290}$ and $pIR_{50}IRSL_{290}$ protocol measurements were both stable, sensitivity between aliquots and samples was more variable for the higher initial temperature protocol than for lower initial temperatures. Aliquots for equivalent dose calculation were accepted according to the criteria described in [53]. The D_e values for each quartz and K-feldspar sample were either averaged (≤6 aliquots) or calculated using the Central Age Model (CAM) of [73] (>6 aliquots; Tables S5 and S6). Given the possibility of residual dose contained within the pIR-IRSL signals [70], we quantified the residual dose on REM3B sample A0376 following bleaching for 300 hours using an LED lamp. These measurements yielded a residual dose of 32.7 ± 4.0 Gy (Table S4). We assumed this value to be representative for loess at the site and therefore subtracted this value from all D_es measured using the pIR-IRSL protocols.

We calculated approximate D_e values for the unprocessed $IRSL_{50}$ measurements by taking the mean of the three aliquot palaeodoses (Table S7).

Equivalent dose estimates are plotted vs. depth for both the profile RP1 and core REM3B in Figure 2. The pIR-IRSL samples in core REM3B are corrected for residual dose (for uncorrected age-depth, see Figure S3).

Preprints (www.preprints.org) | NOT PEER-REVIEWED | Posted: 30 July 2021

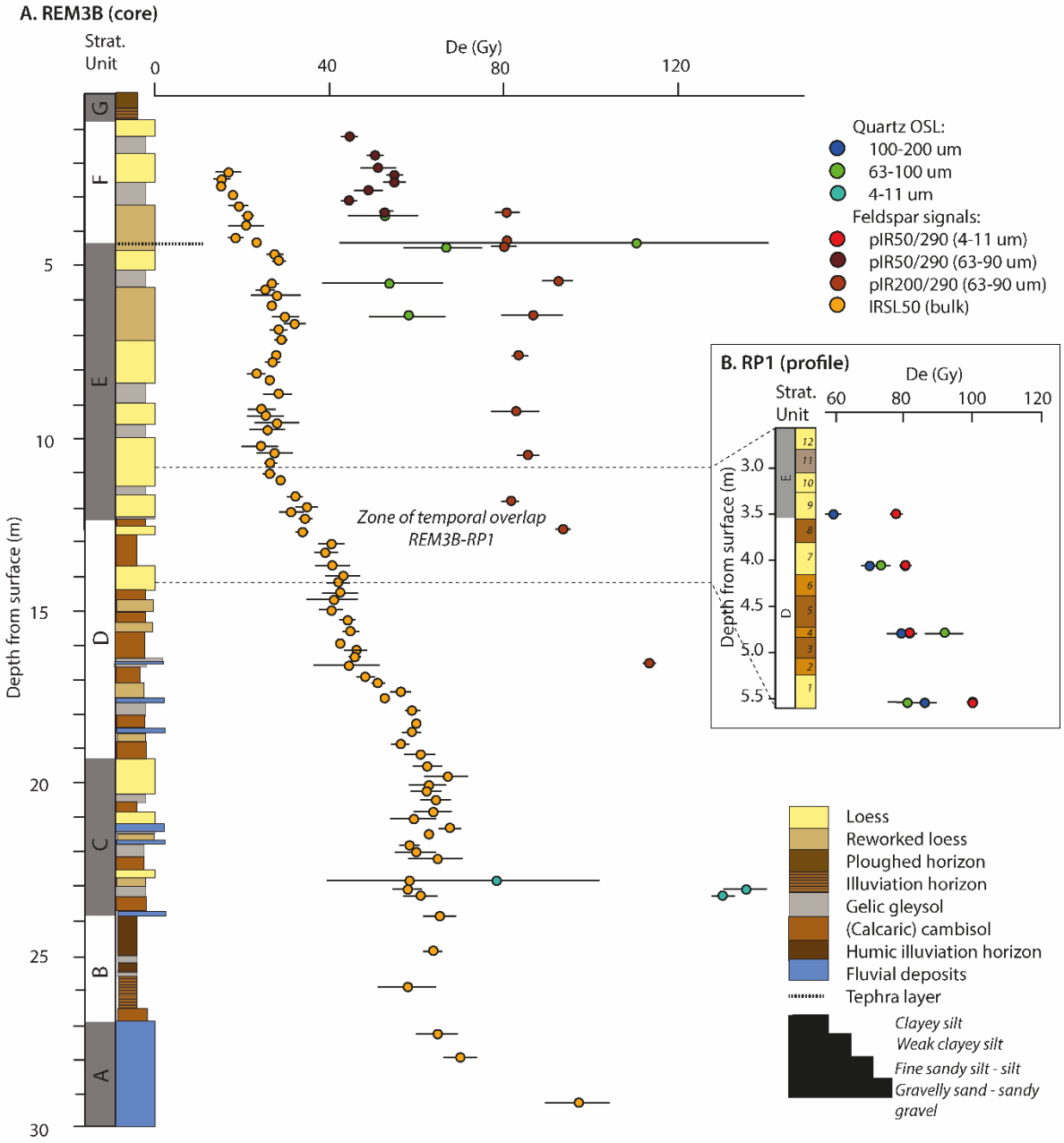

Figure 2. Plots illustrating equivalent dose (1σ error) with depth. (**a**) Equivalent dose vs. depth for the REM3B core, as measured on bulk samples (IR_{50} signal; orange), fine-grained (4-11 μm) and very fine sand-sized (63-100 μm) K-feldspar and quartz aliquots (for respective measurement protocols and mineral fractions, see legend within figure), measured in the MPIC laboratory, Mainz. The stratigraphy and stratigraphic units of the REM3 core [53] are shown for reference; samples from the fluvial sediments at the base of the core are shown for completeness. (**b**) Equivalent dose vs. depth for the profile RP1 [52] based on 63-100 μm and 100-200 μm quartz and 4-11 μm polymineral measurements, measured in the CEZA laboratory, Mannheim. The stratigraphy of the profile is also shown. The zone of temporal overlap between the REM3B core and RP1 profile, determined by detailed stratigraphic correlation in [53], is constrained by dashed lines.

Equivalent dose values broadly increase with depth down the core REM3B, irrespective of measurement protocol (Figure 2A). This is to be expected given that this part of the Schwalbenberg deposit is interpreted to span the last full glacial cycle, from c. 130-0 ka [53]. The IR_{50} measurements on bulk, unprocessed samples also increase with depth and indicate that despite the impure signal measured on this material, it can nevertheless be used to provide a rapidly produced overview scan. Subvertical age-depth relationships can be observed in the stratigraphic units E (and transition to F),

Preprints (www.preprints.org) | NOT PEER-REVIEWED | Posted: 30 July 2021

as well as C-D, suggesting very high sedimentation rates during the deposition of these units. These units have been correlated on the basis of combined lithostratigraphic features and physical characteristics with oxygen isotope stages (OIS) 4 and the early part of OIS 3 (units C-D), and with OIS 2 (units E-F) [53].

There are several notable discrepancies between the different measurement protocol results for the core REM3B. The lower preheat, residual-corrected K-feldspar $pIR_{50}IR_{290}$ protocols yield equivalent doses within error of, and consistent with, the quartz OSL results for the same size fraction (63-90 μm). Where the quartz OSL measurements were paired with the K-feldspar $pIR_{50}IRSL_{290}$, the K-feldspar D_e values are at least 50% greater than those of the quartz. This may be the product of higher residual doses than assumed, incomplete bleaching, or an inappropriate preheat temperature for the K-feldspar samples. However we cannot preclude potential inaccuracies in the quartz as well, such as mixing, incomplete bleaching and multiple signal components, especially since we observe two inverted D_e values at c. 4.5 m depth (Figure 2A), a point at which we observe sedimentary reworking [53]. Unfortunately the lack of available measurable sample precluded a similar comparison for the 4-11 μm quartz OSL measurements in the lower part of the core at c. 23 m depth. However, two of the three samples yield D_e values greater than the K-feldspar estimates further up the core, which is at least consistent with increasing age with depth.

The unprocessed IR_{50} D_e values from core REM3B also consistently increase with depth. We undertook no signal fading measurements on these aliquots and can therefore expect the IR_{50} values to underestimate those from the processed samples. Although the discrepancy between the unprocessed IR_{50} and other measured signals is significant and suggests substantial signal fading, our observations nevertheless indicate that this quick scan approach can be useful to gain an overview of age-depth relationships down long sediment cores [74].

Equivalent dose values increase slightly with depth down profile RP1, irrespective of measurement protocol (Figure 2B). The profile chronology has been interpreted on the basis of combined luminescence and radiocarbon dating to span a relatively short time interval, c. 35-20 ka [53]. Consequently it is to be expected that the D_e values show limited variation. With one exception, the fine-grained polymineral samples yield larger D_e values than for quartz, which is also to be expected given higher internal dose rates in feldspar. There is, however, a discrepancy between the D_e values of the different quartz grain-size fractions. This may reflect the fact that the the quartz signal is approaching saturation at these doses [75, 76]. Furthermore, quartz from Schwalbenberg has previously been observed to contain a substantial contribution of medium component within the overall luminescence signal measured [55]. Whilst these discrepancies hold implications for dating profile RP1 (see discussion in [53]), they do not affect our comparison of test-dose sensitivity here.

3.2. Luminescence sensitivity within profile RP1 and in the zone of temporal overlap between REM3B and RP1

The stratigraphy of profile RP1 has been dated using radiocarbon and luminescence, and is described in detail in [53]. It spans late OIS3 into the last glacial maximum of OIS2, and comprises primary loess in the lowermost excavated c. 20 cm, overlain by c. 1 m of sediment bearing varying degrees of soil development with concomitant high clay proportions. A further c. 20 cm of primary loess overlies this OIS3 soil complex. This is overlain by a thin, clay-rich palaeosol, over which >0.5 m of primary

Preprints (www.preprints.org) | NOT PEER-REVIEWED | Posted: 30 July 2021

loess caps the exposed sequence. A comparable stratigraphic progression is observed in the REM3 cores correlated in [53] to overlap temporally with the RP1 profile (Figure 3).

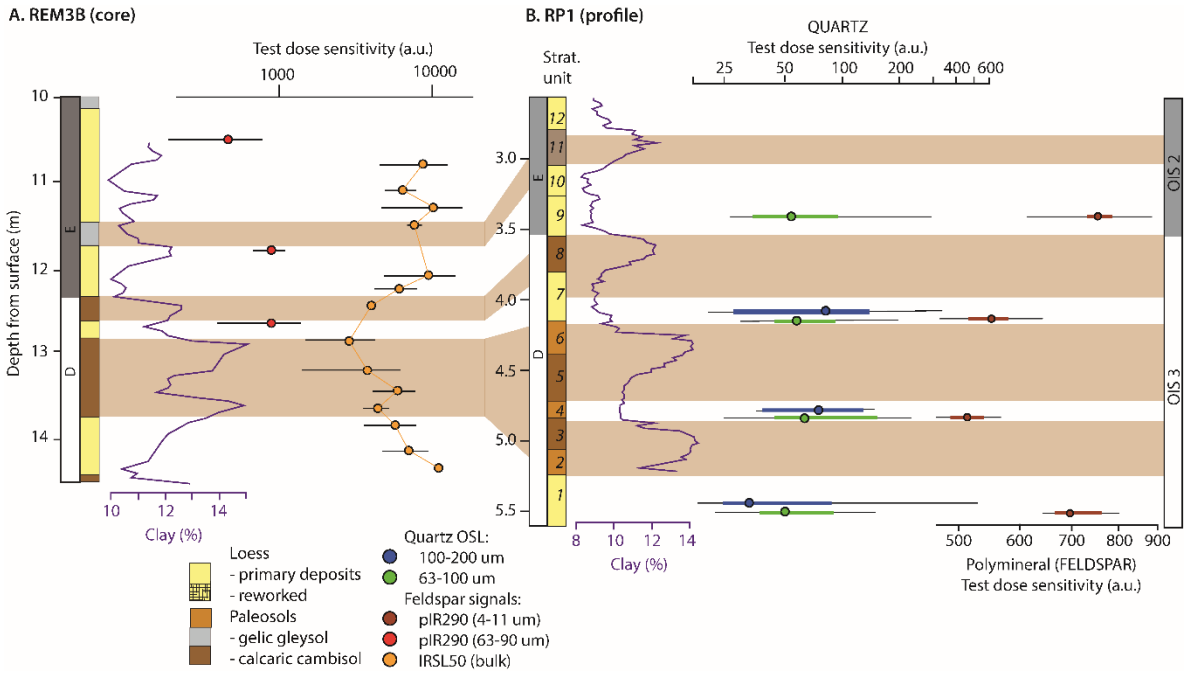

Figure 3. Comparison of luminescence test dose sensitivity (in cts/Gy/s) for the zone of temporal overlap between the REM3B core and RP1 profile. Stratigraphy and clay proportions [53] are shown for reference; gelic gleysol and calcaric cambisol horizons are used for correlation across the figure. (**a**) Down-core test-dose sensitivity at REM3B measured for K-feldspar pIR_{290}, and for bulk sediment using IR_{50}. Error bars indicate standard deviations. (**b**) Down-profile test-dose sensitivity at RP1 based on two quartz size fractions as well as for K-feldspar pIR_{290}. Since 14-24 aliquots were measured for each sample at RP1, sensitivity results are shown as box-plots with the median as a circle.

The luminescence sensitivity arising from the IR_{50} measurements on unprocessed material from core REM3B is illustrated in Figure 3A, along with the $pIR_{200}IR_{290}$ sensitivities on 63-90 μm K-feldspar aliquots of three overlapping samples. A $\log_{10}$ scale is used for the sensitivities, since the unprocessed IR_{50} material is substantially brighter than the processed sample measurements. We observe minimal variation in the sensitivities derived from the samples measured using $pIR_{200}IR_{290}$. By contrast, there is significant variability in the IR_{50} measurements. On the whole, IR_{50} sensitivities increase within the primary loess units, and decrease in the more clay-rich, pedogenic horizons.

The luminescence sensitivity of the four samples collected from profile RP1, measured on 100-200 μm and 63-100 μm quartz and fine-grained polymineral fractions, is shown in Figure 3B. The data are presented as box-plots (medians shown by circles), with respect to stratigraphy and clay concentrations. The Supplementary Information contains more detail on the respective fractions, including the absolute sensitivity values (Table S8), dot plots of all aliquots (Figure S4) and violin and box-plots for the individual fractions (Figures S5-S8). The sensitivities of both quartz size fractions vary minimally within the profile, although we concede that the sampling bias towards primary loess units may have influenced this result. The median values of the coarser (100-200 μm) fraction are slightly higher than for the very fine sand-size (63-90 μm) fraction, with the exception of the lowermost sample. By comparison, the substantially brighter fine-grained (4-11 μm) polymineral (feldspar) fraction varies by c. 50% between the upper- and lowermost samples collected within the

Preprints (www.preprints.org) | NOT PEER-REVIEWED | Posted: 30 July 2021

primary loess (which yield the greatest sensitivity values), and the middle samples from the OIS3 palaeosol package.

Our sensitivity measurements on the unprocessed sample and on 63-90 μm K-feldspar within core REM3B at this depth range facilitate a degree of comparison with the sensitivity characteristics of the fine-grained polymineral samples in the RP1 profile. Despite deriving from different size fractions, the K-feldspar $pIR_{50}IRSL_{290}$ sensitivity values are similar to those observed at the equivalent stratigraphic unit in the RP1 profile. The IR_{50} sensitivity increases in the primary loess horizons and decreases by up to 50% in the more clay-rich palaeosol units, a trend which is echoed in the sensitivity values of the more coarsely sampled fine-grained polymineral measurements from the RP1 profile.

3.3. Luminescence sensitivity down core REM3B

Detailed correlation of a number of cores and profiles in the Schwalbenberg loess deposit established that the REM3 cores (A and B) span the last full glacial cycle [53]. The 27 m REM3 LPS is underlain by c. 3 m of fluvial sediments corresponding to pre-OIS 5. The overlying c. 7.5 m contain predominantly clay-rich pedogenised loess interbedded with thin fluvial units, reworked and primary loess dating to the later stages of OIS 5 through to early OIS 3 (SSU B and C according to [53]). A further c. 7 m of mostly loess, reworked loess and well developed calcaric cambisols overlies that part of the sequence and is interpreted to correspond to OIS 3. The predominantly primary loess of OIS 2, containing several weak palaeosols and reworked loess horizons, comprises the overlying 11.5 m. The sequence is capped by <1 m of modern soil horizon corresponding to OIS 1.

The luminescence sensitivity of all size and mineral fractions measured from REM3B is illustrated in Figure 4 with respect to stratigraphy and clay concentrations (given as % material <2 μm). Given the smaller numbers of aliquots measured relative to the RP1 samples, we present these results as median values (circles) and standard deviations on a logarithmic scale. Absolute test-dose sensitivity values for all measurements run from the REM3B samples are provided in Tables S7 and S9-S11.

Preprints (www.preprints.org) | NOT PEER-REVIEWED | Posted: 30 July 2021

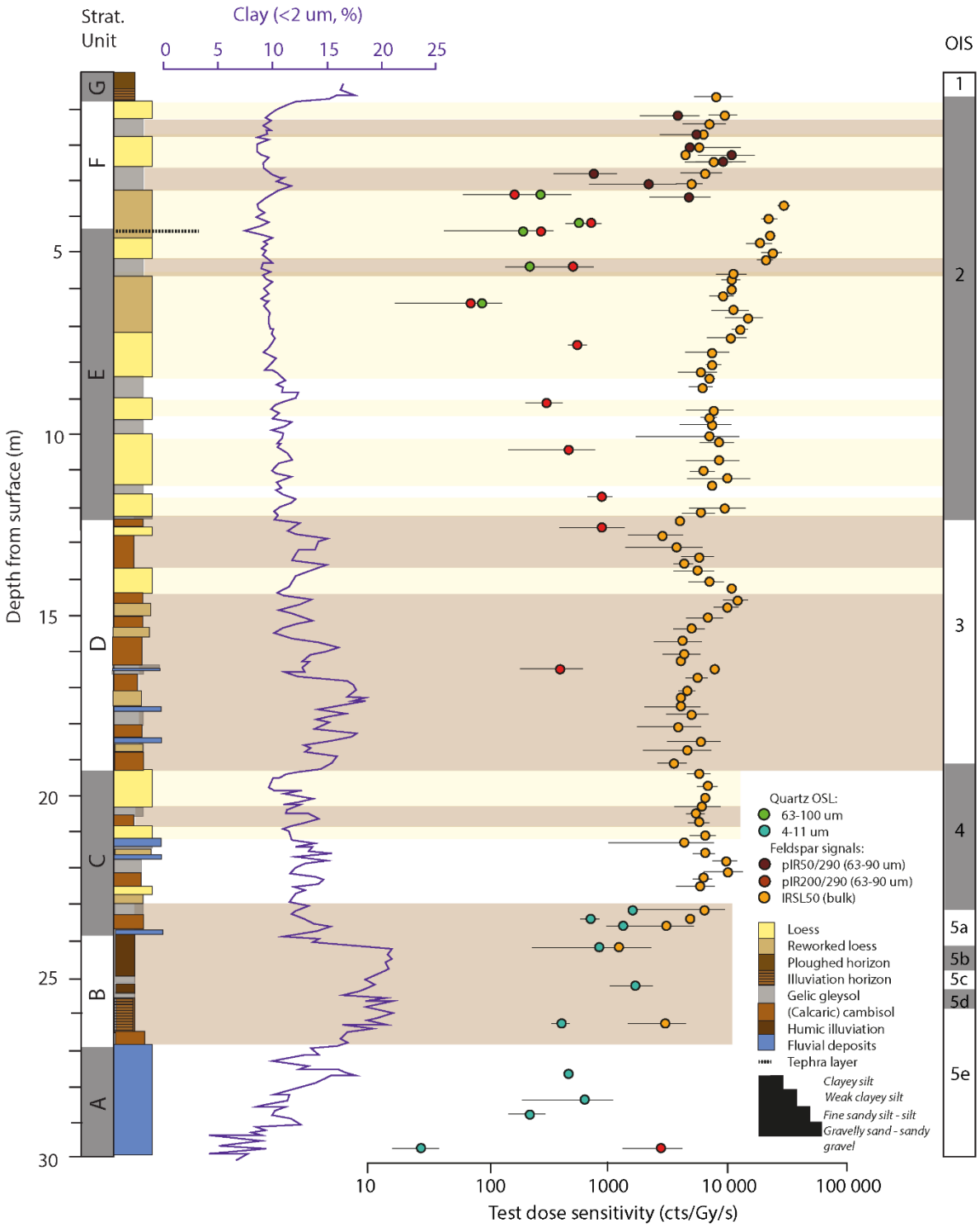

Figure 4. Comparison of luminescence sensitivity with depth down the REM3B core, for quartz OSL, feldspar pIR_{290} and bulk IR_{50} signals. Simplified stratigraphy, the stratigraphic units according to [53] and clay proportions are shown for reference; relevant primary loess units are highlighted in yellow shading and palaeosol horizons in brown.

The unprocessed IR_{50} results provide the most complete and highest resolution dataset from the REM3B core of the protocols used for measurement. As was already observed in the preceding section for the zone of temporal overlap with profile RP1, the IR_{50} sensitivities broadly increase within the primary loess units, and decrease within palaeosol horizons. This trend appears to be reflected in the measurements made using the $pIR_{50}IR_{290}$ protocol on the 63-100 μm K-feldspar

Preprints (www.preprints.org) | NOT PEER-REVIEWED | Posted: 30 July 2021

fraction, and possibly (although less clearly) in the $pIR_{200}IR_{290}$ measurements, although the trend of the latter is less clear. The quartz samples are substantially less sensitive and produce less distinct trends, although the basal fluvial fine-grained quartz yields lower sensitivity values than fine-grained quartz from the overlying pedogenised loessic material.

4. Discussion

4.1. Variability in quartz and feldspar test-dose sensitivity during OIS3

The profile RP1, and subsection of core REM3B which overlaps with it, correspond to OIS3 and the transition to OIS2 [53]. Millennial-scale oscillations in climate are known to have occurred across Europe and the wider North Atlantic region over this period [77-81]. At Schwalbenberg, the impact of short-term climatic oscillations can be identified in the form of sedimentological and chemical changes within the stratigraphy both at RP1 and within the various cores, including REM3, collected from across the loess deposit [53]. The four samples measured from profile RP1 were collected from three clearly identifiable primary loess units (stratigraphic units 9-10, 7 and 1 in [53]; Figure 3) and one from a weakly developed palaeosol within a soil complex (stratigraphic unit 4). This provides us with the opportunity to identify whether OIS3-2 climatic oscillations, which may include variability in dust transport pathways [55, 59, 82] preserved in the form of source changes, are reflected in the luminescence sensitivities of our samples.

The quartz OSL sensitivities of the paired size fractions (63-100 μm and 100-200 μm) lie within error of one another without exception, and yield very little variability (Figure 3B). Standard deviations for the quartz sensitivities are very large irrespective of the number of aliquots measured (for aliquot quantities, see Table S2). As a result, we cannot reliably distinguish any differences in sensitivity of the quartz measured from RP1.

More substantial variability can be observed in the sensitivities derived from the feldspar (polymineral) signals (Figure 3). The 4-11 μm polymineral samples measured using $pIR_{50}IR_{290}$ from profile RP1 appear to yield higher sensitivities for the primary loess units 1 and 9, and lower sensitivities for the palaeosol unit 4 and palaeosol-loess transition 6/7 (Figure 3B). We also observe generally higher sensitivities within primary loess units for the unprocessed IR_{50} signals from core REM3B, and lower sensitivities within pedogenic horizons (Figure 5A). We note that only two processed K-feldspar samples from core REM3B actually overlap with the profile (the uppermost sample in Figure 3A is equivalent to the RP1 stratigraphic unit 12 and cannot be considered as overlapping); the sensitivities of these samples lie within error of one another and yield similar mean values (c. 1000 cts/s/Gy), but the small quantity of samples prevents more robust analysis. We therefore discard these from further consideration. Where there are enough samples measured to facilitate comparison, however, it would appear from our empirical observations that feldspar signal intensities from the processed, and possibly also unprocessed, samples do show a change in characteristics between primary loess and palaeosol units within the Schwalbenberg LPS (Figure 5B). This trend is the inverse of that previously observed for quartz in other LPS across Eurasia [42, 43]. Ours is nevertheless the first empirical study of feldspar signal characteristics. Whilst the mechanisms for feldspar signal sensitivity remain poorly understood [50-52], we posit that one possible explanation for the trends observed here is a change in source (and therefore trajectory) of the mineral dust between the accretionary primary loess, and more stable pedogenic, climatic phases.

Preprints (www.preprints.org) | NOT PEER-REVIEWED | Posted: 30 July 2021

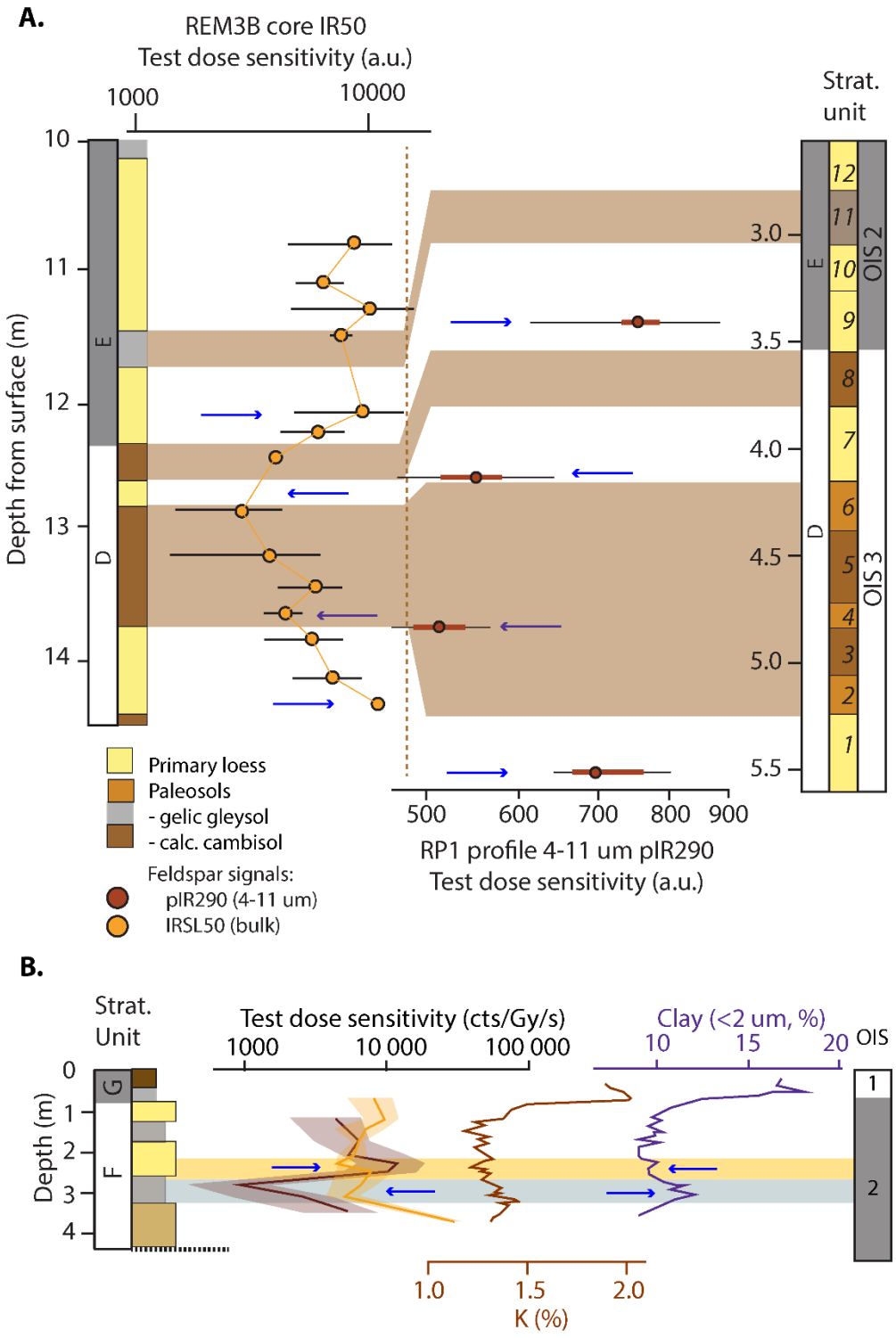

Figure 5. (a) Comparison of bulk IR_{50} and polymineral 4-11 μm $pIR_{50}IR_{290}$ luminescence sensitivity (orange and dark red respectively) for the OIS3-2 overlapping sections of RP1 and REM3B. (b) Comparison of bulk IR_{50} and K-feldspar 63-90 μm $pIR_{50}IR_{290}$ luminescence sensitivity with potassium concentration (brown) and percentage clay (defined as <2 μm; purple), for the upper 4m of the REM3B core. Shading corresponds to 1σ uncertainty range.

4.2 Rapid measurement of luminescence sensitivity in loess: Implications for source variability?

Given the observation that both unprocessed IR_{50} and processed, 4-11 μm $pIR_{50}IR_{290}$ signals in the OIS3-2 period of the RP1 and REM3B records appear to vary between primary loess and palaeosol horizons, we then interrogated the upper 4 m of the REM3B core, where the results of these two

Preprints (www.preprints.org) | NOT PEER-REVIEWED | Posted: 30 July 2021

protocols can be compared. This upper part of the core spans OIS2 and the transition to OIS1 [52], although we did not collect any samples from the Holocene part of the core and therefore can only investigate the glacial maximum period. Nevertheless, the stratigraphy and particularly clay percentages of this part of the core exhibit variations (Figure 5B), most notably oscillations between gelic gleysols and primary loess. Reworked loess is observed below 3.2 m and bracketing the tephra layer.

We observe overall less variability in absolute values of the bulk IR_{50} sensitivities than lower down in the core but nevertheless note increased sensitivity in the loess, and reduced values in the gelic gleysols (Figure 5B). The absolute sensitivity values of the 63-90 μm $pIR_{50}IR_{290}$ measurements are substantially higher than those observed for the finer grained (4-11 μm) fraction from RP1.

Of greatest interest, however, is the fact that both bulk IR_{50} and 63-90 μm $pIR_{50}IR_{290}$ sensitivities yield higher values in the loess and lower values in the gelic gleysols. In addition, the variability in absolute values is greater for the processed, 63-90 μm $pIR_{50}IR_{290}$ aliquots. We propose that both bulk IR_{50} and 63-90 μm $pIR_{50}IR_{290}$ are effectively tapping into the same feldspar signal which is varying between the loess and the gleysols, and that that signal, as suggested above, represents a switch in source - and therefore possibly transport pathway - between the two depositional units, although at this stage we cannot speculate as to where the sources were located. We stress that our observations are empirical and that it is beyond the scope of this study to shed light on the possible mechanisms which may be contributing to the feldspar signal intensity. Furthermore we concede that it is important to consider the mode of pedogenesis within the sediments; gelic gleysols are known to form in this region under partly stagnant conditions overlying the permafrost table and are therefore distinct from calcic cambisols which also occur within the core. Nevertheless, the trends we observe are sufficiently compelling to suggest that sensitivity measurements in feldspar, as previously observed in quartz [42-44], may also provide insights into provenance changes in long sedimentary sequences, although we concede that the mode of pedogenesis may also play a role in feldspar signal sensitivity.

Since we notice effectively the same trends in sensitivity variation for both unprocessed IR_{50} and processed $pIR_{50}IR_{290}$ aliquots (Figure 5), we propose that the rapidly measured bulk IR_{50} signal holds potential as a rapid and simple means to assess variability in sediment source, and thereby changes in dust transport pathways, down LPS and other long sequences (see Section 4.3). We concede that our empirical study does not provide insights into the mechanisms which drive the changes in signal characteristics that we observe here, such as whether higher feldspar sensitivities represent sediments derived from older, metamorphosed or otherwise deformed source rocks. Likewise it may be the case that the process of pedogenesis, which includes weathering of potassium-rich minerals, including feldspar, may have played a role in influencing the signal sensitivity. Nevertheless our observations provide the first basis for future studies investigating the mechanisms driving feldspar sensitivity, and further exploring feldspar characteristics as possible indicators of provenance change.

4.3 Variability in test-dose sensitivity over the last full glacial cycle within core REM3B

Accepting the hypothesis that IR_{50} sensitivity of bulk, unprocessed sediment can be used as a rapid scan for potential provenance, or at least stratigraphic, changes, we then investigated the variability in IR_{50} sensitivity down the REM3B core with respect to stratigraphy, Si/Al ratio as an indicator of provenance change [83], potassium and clay concentration, Ca/Ti ratios and total organic carbon (TOC), as published in [53] (Figure 6). We visually defined an approximate threshold for IR_{50}

Preprints (www.preprints.org) | NOT PEER-REVIEWED | Posted: 30 July 2021

sensitivity – not the mean, since absolute values vary sufficiently that a $\log_{10}$ scale was necessary for presenting the data - above which values were considered "high". We considered 1σ as part of the sensitivity range, since we were conscious of the small numbers of aliquots measured and do not wish to over-interpret the data. We find that in most, but not all, cases, IR_{50} sensitivity exceeds the threshold in samples collected from primary or reworked loess. We likewise find that in most, but not all, cases, IR_{50} sensitivity values from palaeosols or fluvial sediments fell below the defined threshold. We find a striking similarity in trend between IR_{50} sensitivity and the Si/Al ratio, which provides a more established indicator of source change [83]. The data available from the quartz measurements and the K-feldspar $pIR_{200}IR_{290}$ signals are of insufficiently high resolution to conclusively identify trends in sensitivity down the REM3B core (Figure 4), although the fine-grained quartz OSL sensitivities from the basal fluvial sediments are lower than in the LPS part of the sequence. The correlation we observe between IR_{50} sensitivity and Si/Al ratio – including the fact that fluvial sediments unaffected by pedogenesis yield lower sensitivity values - strengthens our hypothesis that changes in IR_{50} sensitivity reflect variability in provenance. Nevertheless we urge caution in this inference since we cannot exclude the possibility that pedogenesis may play a role in influencing feldspar charge transfer.

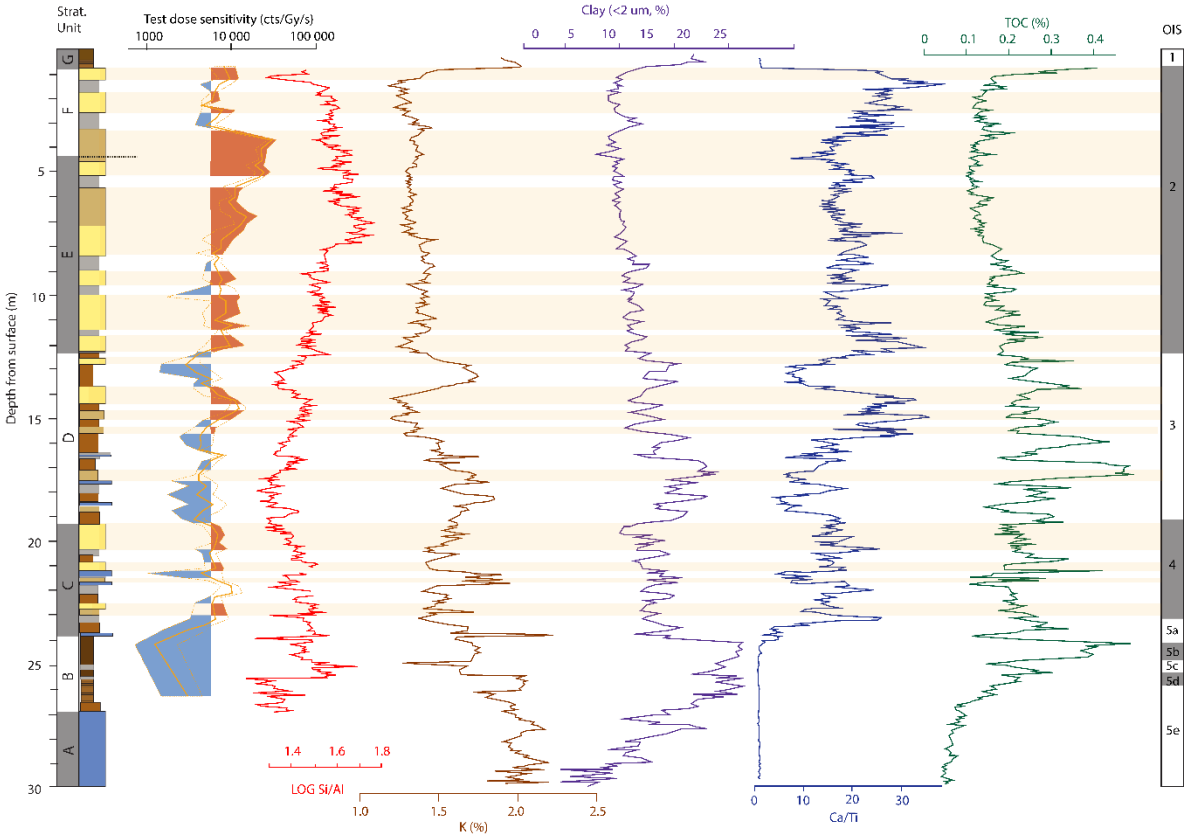

Figure 6. Comparison of bulk IR_{50} luminescence sensitivity (orange solid line representing mean sensitivity, and dotted line representing 1σ range) with Si/Al ratio (scarlet), potassium concentration (dark red), percentage clay (defined as <2 μm; purple), Ca/Ti ratio (dark blue) and total organic carbon (TOC; green), for the REM3 LPS. Primary and reworked loess unit depths are highlighted by beige shading. Where IR_{50} sensitivities exceed the approximately defined threshold and correspond to primary or reworked loess sediments, these are shaded in red; reduced sensitivities below the same threshold which correlate to palaeosols or fluvial sediments are shaded in blue. Stratigraphy and correlation to oxygen isotope stages [52] are shown for reference.

Figure 6 also provides an opportunity to investigate possible correlations between IR_{50} sensitivity and other chemical proxies. There appears to be very little systematic correlation between the IR_{50}

Preprints (www.preprints.org) | NOT PEER-REVIEWED | Posted: 30 July 2021

sensitivity and the Ca/Ti or TOC ratios. It has already been observed from the upper part of the REM3B core that IR_{50} sensitivity appears to have an inverse relationship with clay (<2 μm) concentration (Figure 5B). Observing the variability in sensitivity and clay concentration throughout the entire core (Figure 6), this inverse relationship would appear to hold largely true, although it is not proportional with respect to absolute values. Whether this relationship is mechanistic or simply relates to possible source changes to less sensitive feldspar-bearing sediments during pedogenic phases, which are by nature higher in clay concentration, is unclear at this stage.

A similar anti-correlation can be observed between sensitivity and potassium concentration, whereby potassium proportions increase as IR_{50} sensitivities decrease (Figure 6). Feldspar minerals represent a solid solution with varying proportions of Ca, Al and K within their crystal framework and rarely occur as end-members; along with clay minerals, feldspars represent the main source of K within loessic sediment. It is therefore feasible that the proportion of K down the REM3B core reflects changes in the proportion of K within the feldspars that we are measuring for sensitivity. It has been suggested, in studies aiming to understand the phenomenon of anomalous fading within feldspars for dating, that K concentration may influence the density of available recombination centres [84-87], which might be used as an explanation for the variability that we observe here. However, the structural state of the feldspar is just as important in determining charge transfer [52], and thereby sensitivity, and it is beyond the scope of this study to investigate the interplay between those characteristics within the Schwalbenberg LPS and how these may relate to possible source changes. Notwithstanding these limitations, we propose that the observations of feldspar sensitivity made in this study represent a first step towards exploring the potential of such characteristics as possible indicators of provenance change within sedimentary sequences such as the Schwalbenberg loess.

Supplementary Materials: The following are available online at www.mdpi.com/xxx/s1, Figure S1: Photograph of core REM3A, collected adjacent REM3B, Figure S2: Equivalent dose vs. depth for the different mineral and grain-size fractions measured for profile RP1, Figure S3: Differences in uncorrected equivalent dose vs. depth for the different mineral and grain size fractions down the REM3B core, Figure S4: Test dose sensitivity for the different mineral and grain-size samples measured for profile RP1, Figure S5: Test dose sensitivity for the five very fine sand (63-90 μm) polymineral samples measured from RP1 in this study expressed as violin plot distributions, Figure S6: Test dose sensitivity for the five very fine sand (63-90 μm) K-feldspar samples measured from RP1 in this study expressed as box plots with A) linear and B) logarithmic scale on the x-axis, Figure S7: Box-plots of test-dose sensitivity for the A) 100-200 μm and B) 63-100 μm quartz fraction of samples measured from profile RP1, Figure S8: Box-plots of test-dose sensitivity for the 4-11 μm polymineral fraction of samples measured from profile RP1, Table S1: Overview of luminescence samples collected from the profile RP1, Table S2: Summary of equivalent dose values for the different mineral and grain-size fractions measured for profile RP1, Table S3: Overview of samples from core REM3B measured for this study with respect to measurement protocol, mineral and grain-size fraction, Table S4: Dose recovery and residual dose results for selected samples from core REM3B measured using the $pIR_{200}IR_{290}$ protocol, Table S5: Summary of depths and averaged De values and test dose sensitivity values for the ten fine-grained (4-11μm) and five very fine sand (63-90 μm) quartz OSL samples measured in this study, Table S6: Summary of depths, number of aliquots measured, measurement protocol and averaged uncorrected De values for the 18 very fine sand (63-90μm) K-feldspar samples measured in this study using pIR-IR protocols, Table S7: Summary of depths, averaged De values and test dose sensitivity values for the bulk $IRSL_{50}$ measurements from the REM3B core, Table S8: Summary of depths, average and standard deviation of test dose sensitivity values for the different mineral and grain-size fractions measured for profile RP1, Table S9: Summary of depths, averaged De values and test dose sensitivity values for the ten fine-grained (4-11μm) quartz OSL samples measured in this study, Table S10: Summary of depths, averaged De values and test dose sensitivity values for the five very fine sand (63-90 μm) quartz OSL samples measured in

Preprints (www.preprints.org) | NOT PEER-REVIEWED | Posted: 30 July 2021

this study, Table S11: Summary of depths, averaged uncorrected De values and test dose sensitivity values for the 11 very fine sand (63-90µm) K-feldspar samples measured in this study using the pIR-IR protocols.

Author Contributions: Conceptualization, K.E.F.; methodology, K.E.F.; validation, K.E.F., Z.P. and M.N.; formal analysis, K.E.F., M.N. and S.L.; investigation, K.E.F.; writing—original draft preparation, K.E.F.; writing—review and editing, all authors; funding acquisition, K.E.F., A.V. and P.F. All authors have read and agreed to the published version of the manuscript.

Funding: This research was funded by the German Research Council (DFG), grant number FI1941/5-1 and FI1918/4-1. Additional support for M.N., Z.P., C.P. and A.K.D. was provided by an independent Max Planck Research Group awarded to K.E.F., funded by the Max Planck Society.

Acknowledgments: The authors would like to thank F. Sirocko (University of Mainz) for sharing laboratory facilities.

Conflicts of Interest: The authors declare no conflict of interest.

References

1. Pécsi, M. Loess is not just the accumulation of dust. *Quat. Int.* **1990,** 7-8, 1-21.
2. Pye, K. The nature, origin and accumulation of loess. *Quat. Sci. Rev.* **1995**, 14**,** 653-677.
3. Fitzsimmons, K.E.; Markovic, S.; Hambach, U. Pleistocene environmental dynamics recorded in the loess of the middle and lower Danube basin. *Quat. Sci. Rev.* **2012**, 41**,** 104-118.
4. Liu, T.; Chang, T. The "Huangtu"(loess) of China. In Proceedings of the 6th INQUA Congress, Warsaw, Poland, 1961, **1964**, 4**,** 503-534.
5. Marković, S.B.; Stevens, T.; Kukla, G.J.; Hambach, U.; Fitzsimmons, K.E.; Gibbard, P.; Buggle, B.; Zech, M.; Guo, Z.; Hao, Q.; Wu, H.; O'Hara Dhand, K.; Smalley, I.J.; Ujvari, G.; Sümegi, P.; Timar-Gabor, A.; Veres, D.; Sirocko, F.; Vasiljevic, D.A.; Jary, Z.; Svensson, A.; Jovic, V.; Lehmkuhl, F.; Kovacs, J.; Svircev, Z. Danube loess stratigraphy — Towards a pan-European loess stratigraphic model. *Earth Sci. Rev.* **2015**, 148**,** 228-258.
6. Fitzsimmons, K.E. Reconstructing palaeoenvironments on desert margins: New perspectives from Eurasian loess and Australian dry lake shorelines. *Quat. Sci. Rev.* **2017**, 171**,** 1-19.
7. Buggle, B.; Hambach, U.; Kehl, M.; Markovic, S.B.; Zöller, L.; Glaser, B. The progressive evolution of a continental climate in southeast-central European lowlands during the Middle Pleistocene recorded in loess paleosol sequences. *Geology* **2013,** 41, 771-774.
8. Guo, Z.T.; Ruddiman, W.F.; Hao, Q.Z.; Wu, H.B.; Qiao, Y.S.; Zhu, R.X.; Peng, S.Z.; Wei, J.J.; Yuan, B.Y.; Liu, T.S. Onset of Asian desertification by 22 Myr ago inferred from loess deposits in China. *Nature* **2002,** 416(6877), 159-163.
9. Markovic, S.B.; Hambach, U.; Stevens, T.; Kukla, G.J.; Heller, F.; McCoy, W.D.; Oches, E.A.; Buggle, B.; Zöller, L. The last million years recorded at the Stari Slankamen (Northern Serbia) loess-palaeosol sequence: revised chronostratigraphy and long-term environmental trends. *Quat. Sci. Rev.* **2011**, 30**,** 1142-1154.
10. Fink, J.; Kukla, G.J. Pleistocene climates in central Europe: At least 17 interglacials after the Olduvai event. *Quat. Res.* **1977**, 7(3), 363-371.
11. Licht, A.; Pullen, A.; Kapp, P.; Abell, J.; Giesler, N. Eolian cannibalism: Reworked loess and fluvial sediment as the main sources of the Chinese Loess Plateau. *GSA Bulletin* **2016**, 128(5/6), 944-956.
12. Smalley, I.; O'Hara-Dhand, K.; Wint, J.; Machalett, B.; Jary, Z.; Jefferson, I. Rivers and loess: The significance of long river transportation in the complex event-sequence approach to loess deposit formation. *Quat. Int.* **2009**, 198(1-2), 7-18.

Preprints (www.preprints.org) | NOT PEER-REVIEWED | Posted: 30 July 2021

13. Smalley, I.; Marković, S.B. Controls on the nature of loess particles and the formation of loess deposits. *Quat. Int.* **2019**, 502**,** 160-164.
14. Újvári, G.; Stevens, T.; Svensson, A.; Klötzli, U.S.; Manning, C.; Németh, T.; Kovács, J.; Sweeney, M.R.; Gocke, M.; Wiesenberg, G.L.; Markovic, S.B. Two possible source regions for central Greenland last glacial dust. *Geophys. Res. Lett.* **2015**, 42(23), 2015GL066153.
15. Zaarur, S.; Stein, M.; Adam, O.; Mingram, J.; Liu, J.; Wu, J.; Raveh-Rubin, S.; Erel, Y. Synoptic stability and anomalies in NE China inferred from dust provenance of Sihailongwan maar sediments during the past ~80 kyr. *Quat. Sci. Rev.* **2020**, 239**,** 106279.
16. Buggle, B.; Glaser, B.; Zöller, L.; Hambach, U.; Marković, S.; Glaser, I.; Gerasimenko, N. Geochemical characterization and origin of Southeastern and Eastern European loesses (Serbia, Romania, Ukraine). *Quat. Sci. Rev.* **2008**, 27(9-10), 1058-1075.
17. Obreht, I.; Hambach, U.; Veres, D.; Zeeden, C.; Bösken, J.; Stevens, T.; Marković, S.B.; Klasen, N.; Brill, D.; Burow, C.; Lehmkuhl, F. Shift of large-scale atmospheric systems over Europe during late MIS 3 and implications for Modern Human dispersal. *Sci. Rep.* **2017**, 7**,** 5848.
18. Fitzsimmons, K.E.; Nowatzki, M.; Dave, A.K., Harder, H. Intersections between wind regimes, topography and sediment supply: Perspectives from aeolian landforms in Central Asia. *Palaeogeog. Palaeoclim. Palaeoecol.* **2020**, 540**,** 109531.
19. Li, Y.; Song, Y.; Kaskaoutis, D.G.; Chen, X.; Mamadjanov, Y.; Tan, L. Atmospheric dust dynamics in southern Central Asia: Implications for buildup of Tajikistan loess sediments. *Atmos. Res.* **2019**, 229**,** 74-85.
20. Stuut, J.-B.; Smalley, I.J., O'Hara-Dhand, K. Aeolian dust in Europe: African sources and European deposits. *Quat. Int.* **2009**, 198(1-2), 234-245.
21. Gallet, S.; Jahn, B.M.; Lanoë, B.V.; Dia, A.; Rossello, E. Loess geochemistry and its implications for particle origin and composition of the upper continental crust. *Earth Plan. Sci. Lett.* **1998**, 156(3-4), 157-172.
22. Li, Y.; Song, Y.; Fitzsimmons, K.E.; Chen, X.; Wang, Q.; Sun, H.; Zhang, Z. New evidence for the provenance and formation of loess deposits in the Ili River Basin, Arid Central Asia. *Aeol. Res.* **2018**, 35**,** 1-8.
23. Újvári, G.; Varga, A.; Balogh-Brunstad, Z. Origin, weathering, and geochemical composition of loess in southwestern Hungary. *Quat. Res.* **2008**, 69(3), 421-437.
24. Bird, A.; Stevens, T.; Rittner, M.; Vermeesch, P.; Carter, A.; Andò, S.; Garzanti, E.; Lu, H.; Nie, J.; Zeng, L.; Zhang, H. Quaternary dust source variation across the Chinese Loess Plateau. *Palaeogeog. Palaeoclim. Palaeoecol.* **2015**, 435**,** 254-264.
25. Fenn, K.; Stevens, T.; Bird, A.; Limonta, M.; Rittner, M.; Vermeesch, P.; Andò, S.; Garzanti, E.; Lu, H.; Zhang, H.; Lin, Z. Insights into the provenance of the Chinese Loess Plateau from jointzircon U-Pb and garnet geochemical analysis of last glacial loess. *Quat. Res.* **2018**, 89**,** 645-659.
26. Stevens, T.; Carter, A.; Watson, T.P.; Vermeesch, P.; Andò, S.; Bird, A.F.; Lu, H.; Garzanti, E.; Cottam, M.A.; Sevastjanova, I. Genetic linkage between the Yellow River, the Mu Us desert and the Chinese Loess Plateau. *Quat. Sci. Rev.* **2013**, 78**,** 355-368.
27. Újvári, G.; Varga, A.; Ramos, F.C.; Kovács, J.; Németh, T.; Stevens, T. Evaluating the use of clay mineralogy, Sr–Nd isotopes and zircon U–Pb ages in tracking dust provenance: An example from loess of the Carpathian Basin. *Chem. Geol.* **2012**, 304**,** 83-96.

Preprints (www.preprints.org) | NOT PEER-REVIEWED | Posted: 30 July 2021

28. Újvári, G.; Wegner, W.; Klötzli, U.; Horschinegg, M.; Hippler, D. Sr-Nd-Hf Isotopic Analysis of <10 mg Dust Samples: Implications for Ice Core Dust Source Fingerprinting. *Geochem. Geophys. Geosyst.* **2018**, 19(1), 60-72.
29. Obreht, I.; Zeeden, C.; Hambach, U.; Veres, D.; Marković, S.B.; Bösken, J.; Svirčev, Z.; Bačević, N.; Gavrilov, M.B.; Lehmkuhl, F. Tracing the influence of Mediterranean climate on Southeastern Europe during the past 350,000 years. *Sci. Rep.* **2016**, 6(1), 36334.
30. do Nascimento, D.R.; Sawakuchi, A.O.; Guedes, C.C.; Giannini, P.C.; Grohmann, C.H.; Ferreira, M.P. Provenance of sands from the confluence of the Amazon and Madeira rivers based on detrital heavy minerals and luminescence of quartz and feldspar. *Sed. Geol.* **2015**, 316**,** 1-12.
31. Gray, H.J.; Jain, M.; Sawakuchi, A.O.; Mahan, S.A.; Tucker, G.E. Luminescence as a Sediment Tracer and Provenance Tool. *Rev. Geophys.* **2019**, 57(3), 987-1017.
32. Sawakuchi, A.O.; Rodrigues, F.C.; Mineli, T.D.; Mendes, V.R.; Melo, D.B.; Chiessi, C.M.; Giannini, P.C. Optically Stimulated Luminescence Sensitivity of Quartz for Provenance Analysis. *Methods and Protocols* **2020**, 3**,** 6.
33. Nagashima, K.; Nishido, H.; Kayama, M.; Kurosaki, Y.; Ohgo, S.; Hasegawa, H. Composition of Asian dust from cathodoluminescence spectral analysis of single quartz grains. *Geology* **2017**, 45(10), 879-882.
34. Sun, Y.; Tada, R.; Chen, J.; Chen, H.; Toyoda, S.; Tani, A.; Isozaki, Y.; Nagashima, K.; Hasegawa, H.; Ji, J. Distinguishing the sources of Asian dust based on electron spin resonance signal intensity and crystallinity of quartz. *Atmos. Env.* **2007**, 41(38), 8537-8548.
35. Toyoda, S.; Hattori, W. Formation and decay of the E1′ center and of its precursor. *Appl. Rad. Isotopes* **2000**, 52(5), 1351-1356.
36. Gong, Z.; Sun, J.; Lü, T. Investigating the components of the optically stimulated luminescence signals of quartz grains from sand dunes in China. *Quat. Geochron.* **2015**, 29**,** 48-57.
37. Tsukamoto, S.; Nagashima, K.; Murray, A.S.; Tada, R. Variations in OSL components from quartz from Japan sea sediments and the possibility of reconstructing provenance. *Quat. Int.* **2011**, 234(1-2), 182-189.
38. Fitzsimmons, K.E. An assessment of the luminescence sensitivity of Australian quartz with respect to sediment history. *Geochronometria* **2011**, 38(3), 199-208.
39. Lü, T., Sun, J. Luminescence sensitivities of quartz grains from eolian deposits in northern China and their implications for provenance. *Quat. Res.* **2011**, 76(2), 181-189.
40. Sawakuchi, A.O.; Blair, M.W.; Dewitt, R.; Faleiros, F.M.; Hyppolito, T.; Guedes, C.C. Thermal history versus sedimentary history: OSL sensitivity of quartz grains extracted from rocks and sediments. *Quat. Geochron.* **2011**, 6(2), 261-272.
41. Zheng, C.X.; Zhou, L.P.; Qin, J.T. Difference in luminescence sensitivity of coarse-grained quartz from deserts of northern China. *Rad. Meas.* **2009**, 44(5-6), 534-537.
42. Li, Y.; Zhou, L. Variations of thermally and optically stimulated luminescence sensitivity of loess and pedocomplex samples from southern Tajikistan, Central Asia. *Geochronometria* **2020**, 000010151520150118.
43. Lü, T.; Sun, J.; Li, S.H.; Gong, Z.; Xue L. Vertical variations of luminescence sensitivity of quartz grains from loess/paleosol of Luochuan section in the central Chinese Loess Plateau since the last interglacial. *Quat. Geochron.* **2014**, 22**,** 107-115.
44. Stevens, T.; Adamiec, G.; Bird, A.F.; Lu, H. An abrupt shift in dust source on the Chinese Loess Plateau revealed through high sampling resolution OSL dating. *Quat. Sci. Rev.* **2013**, 82**,** 121-132.
45. Aitken, M.J. *Thermoluminescence dating*. Academic Press: London, UK, 1985.

Preprints (www.preprints.org) | NOT PEER-REVIEWED | Posted: 30 July 2021

46. Haase, D.; Fink, J.; Haase, G.; Ruske, R.; Pécsi, M.; Richter, H.; Altermann, M.; Jäger, K.D. Loess in Europe--its spatial distribution based on a European Loess Map, scale 1:2,500,000. *Quat. Sci. Rev.* **2007**, 26(9-10), 1301-1312.
47. Rousseau, D.-D.; Boers, N.; Sima, A.; Svensson, A.; Bigler, M.; Lagroix, F.; Taylor, S.; Antoine, P. (MIS3 & 2) millennial oscillations in Greenland dust and Eurasian aeolian records – A paleosol perspective. *Quat. Sci. Rev.* **2017**, 169**,** 99-113.
48. Lehmkuhl, F.; Nett, J.J.; Pötter, S.; Schulte, P.; Sprafke, T.; Jary, Z.; Antoine, P.; Wacha, L.; Wolf, D.; Zerboni, A.; Hošek, J. Loess landscapes of Europe–Mapping, geomorphology, and zonal differentiation. *Earth Sci. Rev.* **2020**, 103496.
49. Jain, M.; Ankjærgaard, C. Towards a non-fading signal in feldspar: Insight into charge transport and tunnelling from time-resolved optically stimulated luminescence. *Rad. Meas.* **2011**, 46(3), 292-309.
50. Pagonis, V.; Jain, M.; Murray, A.S.; Ankjærgaard, C.; Chen, R. Modeling of the shape of infrared stimulated luminescence signals in feldspars. *Rad. Meas.* **2012**, 47(9), 870-876.
51. Guralnik, B.; Li, B.; Jain, M.; Chen, R.; Paris, R.B.; Murray, A.S.; Li, S.H.; Pagonis, V.; Valla, P.G.; Herman F. Radiation-induced growth and isothermal decay of infrared-stimulated luminescence from feldspar. *Rad. Meas.* **2015**, 81**,** 224-231.
52. Riedesel, S.; Bell, A.M.; Duller, G.A.; Finch, A.A.; Jain, M.; King, G.E.; Pearce, N.J.; Roberts, H.M. Exploring sources of variation in thermoluminescence emissions and anomalous fading in alkali feldspars. *Rad. Meas.* **2021**, 141**,** 106541.
53. Fischer, P.; Jöris, O.; Fitzsimmons, K.E.; Vinnepand, M.; Prud'Homme, C.; Schulte, P.; Hatté, C.; Hambach, U.; Lindauer, S.; Zeeden, C.; Peric, Z. Millennial-scale terrestrial ecosystem responses to Upper Pleistocene climatic changes: 4D-reconstruction of the Schwalbenberg Loess-Paleosol-Sequence (Middle Rhine valley, Germany). *Catena* **2021**, 196**,** 104913.
54. Vinnepand, M.; Fischer, P.; Fitzsimmons, K.E.; Thornton, B.; Fiedler, S.; Vött, A. Combining Inorganic and Organic Carbon Stable Isotope Signatures in the Schwalbenberg Loess-Palaeosol-Sequence Near Remagen (Middle Rhine Valley, Germany). *Frontiers in Earth Sci.* **2020**, 8**,** 276.
55. Klasen, N.; Fischer, P.; Lehmkuhl, F.; Hilgers, A. Luminescence dating of loess deposits from the Remagen-Schwalbenberg site, western Germany. *Geochronometria* **2015**, 42**,** 67-77.
56. Schirmer, W.; Ikinger, A.; Nehring, F. Die terrestrischen Böden im Profil Schwalbenberg/Mittelrhein. (Terrestrial soils of the Schwalbenberg profile/Middle Rhine). *Mainzer Geowiss. Mitteilungen* **2012**, 40**,** 53-78.
57. Schirmer, W. Late Pleistocene loess of the lower Rhine. *Quat. Int.* **2016**, 411**,** 44-61.
58. Bibus, E. Zur Relief-, Boden-und Sedimententwicklung am unteren Mittelrhein. *Frankfurter Geowiss. Arbeiten* **1980**, D1.
59. Profe, J.; Zolitschka, B.; Schirmer, W.; Frechen, M.; Ohlendorf C. Geochemistry unravels MIS 3/2 paleoenvironmental dynamics at the loess–paleosol sequence Schwalbenberg II, Germany. *Palaeogeog. Palaeoclim. Palaeoecol.* **2016**, 459**,** 537-551.
60. Schirmer, W. Würmzeitliche Böden am Mittelrhein. In Program and Exkursionsführer, Proceedings of the 10. Tagung des AK Paläoböden der DBG, Germany, 1991.
61. Schirmer, W. Eine Klimakurve des Oberpleistozäns aus dem rheinischen Löss. *Eiszeit. und Gegenwart* **2000**, 50(1), 25-49.
62. Boenigk, W.; Frechen, M. The Pliocene and Quaternary fluvial archives of the Rhine system. *Quat. Sci. Rev.* **2006**, 25(5-6), 550-574.

Preprints (www.preprints.org) | NOT PEER-REVIEWED | Posted: 30 July 2021

63. Frechen, M.; Schirmer, W. Luminescence chronology of the Schwalbenberg II loess in the Middle Rhine valley. *E&G Quat. Sci. J.* **2011**, 60(1), 78-89.
64. Schiermeyer, J. *Würmzeitliche Lößmollusken aus der Eifel.* Universität Düsseldorf: Düsseldorf, 2002.
65. App, V. Die altsteinzeitliche Fundstelle auf dem Schwalbenberg bei Remagen. *Berichte zur Archäologie an Mittelrhein und Mosel* **1995**, 4**,** 11-136.
66. Lang, A.; Lindauer, S.; Kuhn, R.; Wagner, G.A. Procedures used for optically and infrared stimulated luminescence dating of sediments in Heidelberg. *Ancient TL* **1996**, 14(3), 7-11.
67. Bøtter-Jensen, L. Luminescence techniques: instrumentation and methods. *Rad. Meas.* **1997**, 27**,** 749-768.
68. Murray, A.S.; Wintle, A.G. Luminescence dating of quartz using an improved single-aliquot regenerative-dose protocol. *Rad. Meas.* **2000**, 32(1), 57-73.
69. Murray, A.S.; Wintle, A.G. The single aliquot regenerative dose protocol: potential for improvements in reliability. *Rad. Meas.* **2003**, 37(4-5), 377-381.
70. Buylaert, J.-P.; Jain, M.; Murray, A.S.; Thomsen, K.J.; Thiel, C.; Sohbati, R. A robust feldspar luminescence dating method for Middle and Late Pleistocene sediments. *Boreas* **2012**, 41(3), 435-451.
71. Perić, Z.; Adolphi, E.L.; Stevens, T.; Újvári, G.; Zeeden, C.; Buylaert, J.P.; Marković, S.B.; Hambach, U.; Fischer, P.; Schmidt, C.; Schulte, P. Quartz OSL dating of late quaternary Chinese and Serbian loess: A cross Eurasian comparison of dust mass accumulation rates. *Quat. Int.* **2019**, 502(A), 30-44.
72. Timar, A.; Vandenberghe, D.; Panaiotu, E.C.; Panaiotu, C.G.; Necula, C.; Cosma, C. Optical dating of Romanian loess using fine-grained quartz. *Quat. Geochron.* **2010**, 5(2-3), 143-148.
73. Galbraith, R.F.; Roberts, R.G.; Laslett, G.M.; Yoshida, H.; Olley, J.M. Optical dating of single and multiple grains of quartz from Jinmium rock shelter, northern Australia. Part 1, Experimental design and statistical models. *Archaeometry* **1999**, 41**,** 339-364.
74. Preusser, F. Bulk sediment IRSL screening applied for high-resolution and fast age assessment of fluvial deposits in the Upper Rhine Plain. In Proceedings of the German Luminescence and Electron Spin Resonance Dating (DLED) Conference, Bingen, Germany, 8-10 November 2019.
75. Anechitei-Deacu, V.; Timar-Gabor, A.; Thomsen, K.J.; Buylaert, J.P.; Jain, M.; Bailey, M.; Murray, A.S. Single and multi-grain OSL investigations in the high dose range using coarse quartz. *Rad. Meas.* **2018**, 120, 124-130.
76. Timar Gabor, A.; Vandenberghe, D.A.; Vasiliniuc, S.; Panaoitu, C.E.; Panaiotu, C.G.; Dimofte, D.; Cosma, C. Optical dating of Romanian loess: A comparison between silt-sized and sand-sized quartz. *Quat. Int.* **2011**, 240(1-2), 62-70.
77. Fuhrmann, F.; Diensberg, B.; Gong, X.; Lohmann, G.; Sirocko, F. Aridity synthesis for eight selected key regions of the global climate system during the last 60 000 years. *Clim. Past* **2020**, 16(6), 2221-38.
78. Fuhrmann, F.; Seelos, K.; Sirocko, F. Eolian sedimentation in central European Auel dry maar from 60 to 13 ka. *Quat. Res.* **2021**, *101*, 4-12.
79. Sirocko, F.; Knapp, H.; Dreher, F.; Förster, M.W.; Albert, J.; Brunck, H.; Veres, D.; Dietrich, S.; Zech, M.; Hambach, U.; Röhner, M. The ELSA-Vegetation-Stack: Reconstruction of Landscape Evolution Zones (LEZ) from laminated Eifel maar sediments of the last 60,000 years. *Global Planet. Change* **2016**, 142, 108-35.
80. Zeeden, C.; Hambach, U.; Veres, D.; Fitzsimmons, K.; Obreht, I.; Bösken, J.; Lehmkuhl, F. Millennial scale climate oscillations recorded in the Lower Danube loess over the last glacial period. *Palaeogeog. Palaeoclim. Palaeoecol.* **2018**, 509, 164-81.

Preprints (www.preprints.org) | NOT PEER-REVIEWED | Posted: 30 July 2021

81. Rasmussen, S.O.; Bigler, M.; Blockley, S.P.; Blunier, T.; Buchardt, S.L.; Clausen, H.B.; Cvijanovic, I.; Dahl-Jensen, D.; Johnsen, S.J.; Fischer, H.; Gkinis, V. A stratigraphic framework for abrupt climatic changes during the Last Glacial period based on three synchronized Greenland ice-core records: refining and extending the INTIMATE event stratigraphy. *Quat. Sci. Rev.* **2014**, 106, 14-28.

82. Schaffernicht, E.J.; Ludwig, P.; Shao Y. Linkage between dust cycle and loess of the Last Glacial Maximum in Europe. *Atmos. Chem. Phys.* **2020**, 20(8), 4969-86.

83. Vinnepand, M.; Fischer, P.; Zeeden, C.; Schulte, P.; Fiedler, S.; Jöris, O.; Hambach, U.; Fitzsimmons, K.E.; Prud'homme, C.; Peric, Z.; Schirmer, W.; Lehmkuhl, F.; Vött, A. Decoding multivariate geochemical signatures of the Upper Pleistocene Schwalbenberg loess-palaeosol sequence - implications on changes of source areas and weathering intensities. *Catena*, **in review**.

84. Huntley, D.J.; Lian, O.B. Some observations on tunnelling of trapped electrons in feldspars and their implications for optical dating. *Quat. Sci. Rev.* **2006**, *25*(19-20), 2503-2512.

85. Valla, P.G.; Lowick, S.E.; Herman, F.; Champagnac, J.D.; Steer, P.; Guralnik, B. Exploring IRSL50 fading variability in bedrock feldspars and implications for OSL thermochronometry. *Quaternary Geochronology* **2016**, *36*, 55-66.

86. Trauerstein, M.; Lowick, S.; Preusser, F.; Rufer, D.; Schlunegger, F. Exploring fading in single grain feldspar IRSL measurements. *Quat. Geochron.* **2012**, 10, 327-333.

87. Visocekas, R.; Zink, A. Tunneling afterglow and point defects in feldspars. *Rad. Effects and Defects in Solids* **1995**, 134(1-4), 265-272.